Synchrotron and neutron powder diffraction study of phase transition in weberite-type Nd_3NbO_7 and La_3NbO_7

Lu Cai [a,*], Juan C. Nino [b]

[a] Spallation Neutron Source, Oak Ridge National Laboratory, PO Box 2008 MS6454, Oak Ridge, TN 37831, USA
[b] Department of Materials Science and Engineering, University of Florida, Gainesville, FL 32611, USA

ARTICLE INFO

ABSTRACT

La_3NbO_7 and Nd_3NbO_7 are insulating compounds that have an orthorhombic weberite-type crystal structure and undergo a phase transition at about 360 and 450 K, respectively. The nature of the phase transitions was investigated via heat capacity measurements, synchrotron X-ray and neutron diffraction experiments. It is here shown that above the phase transition temperature, the compounds possess a weberite-type structure described by space group $Cmcm$ (No. 63). Below the phase transition, the high temperature phase transforms into a weberite-type structure with space group $Pmcn$ (No. 62). The phase transformation primarily involves the off-center shifting of Nb^{5+} ions inside the NbO_6 octahedra, combined with shifts of one third of the Ln^{3+} ($Ln^{3+} = La^{3+}$ and Nd^{3+}) ions at the center of the LnO_8 polyhedra towards off-center positions. The phase transition was also proven to have great impacts on the dielectric properties.

© 2011 Elsevier Inc. All rights reserved.

1. Introduction

Weberite-type Ln_3BO_7 compounds (where Ln^{3+} is a rare earth element, and B is Os^{5+}, Re^{5+}, Ru^{5+}, Re^{5+}, Mo^{5+}, Ir^{5+}, Sb^{5+}, Nb^{5+} or Ta^{5+}) attract great attention because they exhibit interesting properties including magnetic [1–8], dielectric [9,10] as well as photocatalytic activity [11,12]. The crystal structure of these compounds is also interesting due to its close relationships to the pyrochlore and weberite structures ($A_2B_2O_7$) [13,14]. The space group of these compounds was first assigned as $Pnma$ (No. 62) [15,16]. However, when the crystal structure was first reported by Rossell [17], the space group $Cmcm$ (No. 63) was used. Rossell's description of the crystal structure as well as the space group $Cmcm$ was then the prototype widely accepted for Ln_3BO_7-type compounds including Ln_3RuO_7 ($Ln^{3+} = La^{3+}$, Pr^{3+}, Nd^{3+}, and Sm^{3+}) [6,18–27], Ln_3TaO_7 ($Ln^{3+} = La^{3+}$, Pr^{3+}, and Nd^{3+}) [1,28,29], Ln_3IrO_7 ($Ln^{3+} = Pr^{3+}$, Nd^{3+}, Sm^{3+}, and Eu^{3+}) [5,30,31], and Ln_3ReO_7 ($Ln^{3+} = Pr^{3+}$, Nd^{3+}, Sm^{3+}, Gd^{3+}, Tb^{3+}, and Dy^{3+}) [3,4,8,32]. Rossell et al. [17,33] also commented on the unexpected very weak $h0l$ reflections with odd l in Nd_3NbO_7, which are forbidden in $Cmcm$. Kahnharari et al. [34] claimed the very weak forbidden reflections could not be neglected and based on single crystal diffraction data of La_3NbO_7 assigned it the space group $Pnma$. Later, Doi et al. [35] also observed forbidden

reflections of $Cmcm$ from powder X-ray and refined the crystal structure of Nd_3NbO_7 using the space group $Pnma$. This discrepancy found in literature can be understood recognizing that it may be challengeable to distinguish the weak reflections, which are critical for space group determination, from the background by conventional $CuK\alpha$ X-ray diffraction (XRD) alone. Therefore, synchrotron powder diffraction experiments have been performed to clarify the space group at 11-BM of Advanced Photon Source in Argonne National Laboratory, one of the highest resolution powder diffractometer.

In addition, an interesting phase transition has been observed in these two compounds primarily through heat capacity measurements. It has been claimed that the phase transition is due to the displacement of atoms with no change in crystal system and no "appreciable" change in lattice parameters based on XRD [36]. In fact, phase transitions are commonly observed in the Ln_3BO_7 family of compounds. Consequently, there have been several studies focusing in the crystallography of Ln_3IrO_7 [31], Ln_3MoO_7 [37–40], Ln_3OsO_7 [41], Ln_3RuO_7 [42,43], and Gd_3NbO_7 [44]. For example, it has been reported that the phase transition in Sm_3OsO_7, Eu_3OsO_7, and Gd_3OsO_7 involved the change from space group $P2_1nb$ (No. 33) to $Cmcm$ on heating, while maintaining an orthorhombic lattice [41]. Nd_3RuO_7 undergoes a phase transition from monoclinic ($P2_1/m$, No. 11) with $\beta = 90.008°$ to orthorhombic ($Cmcm$) [25].

Given this, it is reasonable to assume that above the phase transition temperature the space group of La_3NbO_7 and Nd_3NbO_7 is $Cmcm$, which has the highest symmetry among all space groups

* Corresponding author.
  E-mail address: cail@ornl.gov (L. Cai).

reported for Ln_3BO_7 compounds. However, the origin of the phase transition and in particular the crystallography of the low temperature phase for these compounds remains unclear. Therefore, neutron powder diffraction as a function of temperature is used to investigate the crystal structure (including space group) of Nd_3NbO_7 and La_3NbO_7 below and above the phase transition temperature.

2. Experimental procedure

Polycrystalline specimens of Ln_3NbO_7 ($Ln^{3+}=La^{3+}$ and Nd^{3+}) were synthesized by conventional solid oxide reaction from a stoichiometric mixture of Ln_2O_3 (Alfa, 99.9%) and Nb_2O_5 (Alfa, 99.9985%). Nd_2O_3 and Nb_2O_5 were mixed by wet ball-milling for

Fig. 1. Heat capacity of La_3NbO_7 and Nd_3NbO_7.
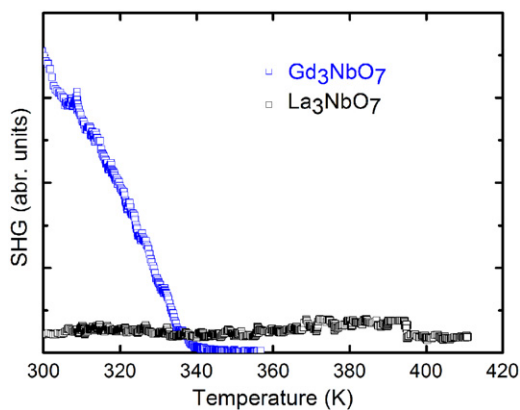
Fig. 2. SHG of La_3NbO_7 and Gd_3NbO_7 [44].

24 h and then subsequently dried in the oven at 393 K for 16 h. The dried powder was then ground and sieved through a 212 μm mesh. The powder was then placed in an alumina crucible for calcination at 1773 K. Multiple calcinations were used and $CuK\alpha$ radiation X-ray diffraction (XRD) was collected after each calcination at room temperature to verify phase formation. Equilibrium was presumed when no further changes could be detected. The synchrotron X-ray diffraction was performed using the 11-BM high resolution powder diffractometer at the Advanced Photon Source, Argonne National Laboratory. The neutron powder diffraction data was collected using the HB-2A neutron powder diffractometer at the High Flux Isotope Reactor, Oak Ridge National Laboratory.

The phase pure powders were then uniaxially pressed into cylindrical-shaped pellets (13 mm or 7 mm in diameter and approximately 1 mm thickness) using polyvinyl alcohol (∼1–3 wt%) as a binder under a pressure of 150 MPa. A binder burn-out step at 723 K for 2 h was followed by sintering in air at 1873 K for 8 h. The heat capacity measurement of Nd_3NbO_7 and La_3NbO_7 pellets was conducted using a differential scanning calorimetrer (Seiko Instrument, Inc.) following ASTM E 1269-05 [45]. The measurement was done in nitrogen atmosphere using synthetic sapphire disk as a standard from 160 to 673 K.

To prepare parallel plate capacitors, Au/Pd or Au electrodes were sputtered on both sides of the polished pellets followed by a painted coat of air-dried Ag-paste. Dielectric properties were
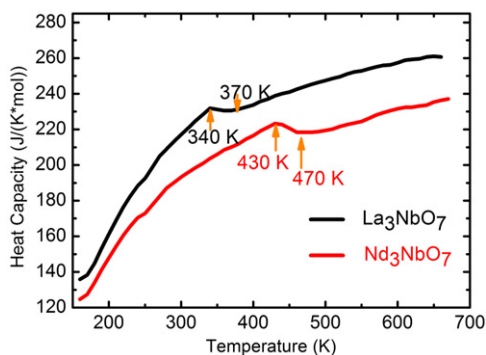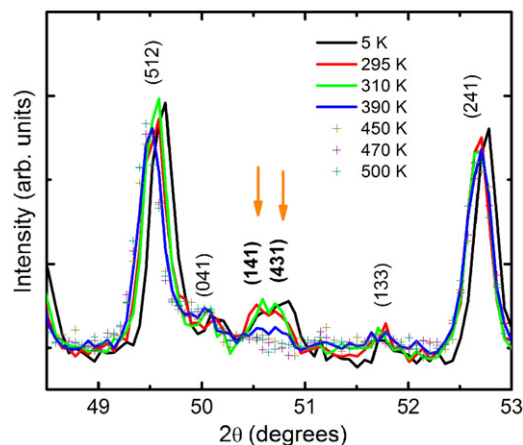

Fig. 4. Neutron diffraction patterns at different temperatures ($\lambda=1.5378$ Å). The patterns below the phase transition temperature are plotted in lines. The patterns above the phase transition temperature are plotted in scattered points. Two extra reflections at the low temperature phase are pointed by the arrows.
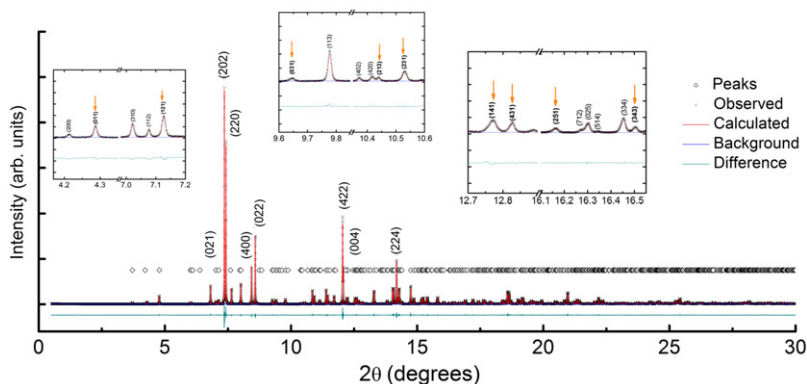

Fig. 3. Synchrotron diffraction of Nd_3NbO_7 at room temperature ($\lambda=0.40092$ Å) including the details of the forbidden peaks by $Cmcm$. The forbidden peaks are pointed by the arrows. Diamond symbols indicate the less intense peaks, which are associate with the Nd_3NbO_7 structure but not indexed. The Rietveld method was used to refine the pattern as shown in the red lines. (For interpretation of the references to color in this figure legend, the reader is referred to the web version of this article.)

Table 1

Crystal data of Nd_3NbO_7 for the low temperature phase (that at 100 K is from synchrotron diffraction). For neutron diffraction data, there are total 1832 reflections and 64 parameters refined. The wavelength is 1.5378 Å. The refined 2θ range is 10–130°. For synchrotron diffraction, there are total 29501 reflections and 62 parameters refined. The wavelength is 0.400919 Å. The refined 2θ is 0.5–29.999°.

5 K
$R_w=8.06\%$, $R_p=6.12\%$, $\chi^2=2.872$
Space group: *Pmcn*
10.8815(2) Å, 7.5208(2) Å, 7.6162(1) Å

	Wyckoff	x	y	z	U_{iso}
Nb	4*c*	0.25	0.2548(9)	0.027(15)	0.0068(9)
Nd1	4*c*	0.25	0.7776(7)	0.0102(10)	0.0057(5)
Nd2	8*d*	0.4773(2)	0.4540(4)	0.2504(9)	0.0119(10)
O1	8*d*	0.9652(7)	0.8717(5)	0.9504(6)	0.0066(10)
O1′	8*d*	0.3851(7)	0.4144(7)	0.9594(10)	0.0286(15)
O2	8*d*	0.3817(4)	0.7267(5)	0.2563(12)	0.0119(9)
O3	4*c*	0.25	0.3249(7)	0.253(2)	0.0131(12)

100 K
Space group: *Pmcn*
10.8930(2) Å, 7.5238(2) Å, 7.6179(2) Å
$R_w=15.31\%$, $R_p=15.31\%$, $\chi^2=9.398$

	Wyckoff	x	y	z	U_{iso}
Nb	4*c*	0.25	0.2526(1)	0.0043(3)	0.0020(2)
Nd1	4*c*	0.25	0.7794(1)	0.0082(1)	0.0022(1)
Nd2	8*d*	0.47689(3)	0.45359(5)	0.25164(9)	0.00132(7)
O1	8*d*	0.8722(5)	0.9475(6)	0.9653(8)	0.005(1)
O1′	8*d*	0.3828(5)	0.4128(6)	0.9626(8)	0.012(1)
O2	8*d*	0.3821(4)	0.7264(6)	0.2529(11)	0.0007(10)
O3	4*c*	0.25	0.3227(8)	0.2472(13)	0.003(2)

295 K
Space group: *Pmcn*
10.8988(3) Å, 7.5285(2) Å, 7.6270(2) Å
$R_w=7.94\%$, $R_p=6.01\%$, $\chi^2=2.845$

	Wyckoff	x	y	z	U_{iso}
Nb	4*c*	0.25	0.2542(11)	−0.0029(11)	0.006(1)
Nd1	4*c*	0.25	0.7734(8)	0.0093(10)	0.0093(11)
Nd2	8*d*	0.4779(3)	0.4551(4)	0.2522(10)	0.0072(6)
O1	8*d*	0.8718(6)	0.9502(7)	0.9680(8)	0.013(1)
O1′	8*d*	0.3826(7)	0.4208(9)	0.9561(9)	0.019(1)
O2	8*d*	0.3823(4)	0.7267(5)	0.2462(13)	0.0087(10)
O3	4*c*	0.25	0.3236(8)	0.252(2)	0.0115(12)

310 K
Space group: *Pmcn*
10.8971(3) Å, 7.5292(2) Å, 7.6257(2) Å
$R_w=8.14\%$, $R_p=6.29\%$, $\chi^2=2.933$

	Wyckoff	x	y	z	U_{iso}
Nb	4*c*	0.25	0.2539(12)	0.005(2)	0.012(1)
Nd1	4*c*	0.25	0.7747(10)	0.0085(12)	0.016(1)
Nd2	8*d*	0.4782(3)	0.4542(4)	0.2506(12)	0.0111(8)
O1	8*d*	0.8727(7)	0.9493(8)	0.9633(10)	0.011(1)
O1′	8*d*	0.3829(8)	0.4193(9)	0.9538(13)	0.034(2)
O2	8*d*	0.3827(4)	0.7261(6)	0.255(2)	0.014(1)
O3	4*c*	0.25	0.3245(8)	0.255(2)	0.018(1)

390 K
Space group: *Pmcn*
10.9048(3) Å, 7.5262(2) Å, 7.6342(2) Å
$R_w=8.96\%$, $R_p=6.80\%$, $\chi^2=7.129$

	Wyckoff	x	y	z	U_{iso}
Nb	4*c*	0.25	0.2501(15)	0.003(2)	0.017(1)
Nd1	4*c*	0.25	0.7658(14)	0.009(2)	0.0238(17)
Nd2	8*d*	0.4781(3)	0.4535(5)	0.2532(14)	0.0153(7)
O1	8*d*	0.8720(8)	0.9498(9)	0.9650(13)	0.019(2)
O1′	8*d*	0.3834(11)	0.4204(12)	0.9610(17)	0.041(3)
O2	8*d*	0.3828(5)	0.7268(7)	0.250(2)	0.020(2)
O3	4*c*	0.25	0.3218(9)	0.249(3)	0.026(2)

measured using an Agilent 4980 A LCR meter over a frequency range of 1 kHz–1 MHz. The measurements were computer controlled with samples inside Delta 9023 oven from 113 to 500 K (liquid nitrogen cooled) or in a closed cycle cryogenic workstation (CTI-Cryogenics, Model 22) in the temperature range of 20–295 K.

The second harmonic generation (SHG) signal was measured on sintered pellets, which were polished progressively with smaller sizes of alumina powder and finally submicron size colloidal silica. The laser source was an amplified Ti:sapphire laser with 1 kHz repetition rate, 800 nm wavelength and 130 fs pulse width. The signal was collected using photomultiplier tube and lock-in amplifier to reduce noise. The laser was incident at 45° to the sample surface.

3. Results and discussion

3.1. Heat capacity and second harmonic generation measurements

Klimenko et al. [36] first measured the heat capacity of Nd_3NbO_7 and La_3NbO_7 from 295 to 1100 K. In this study, the heat capacity was re-measured. The measuring temperature was extended down to 170 K as shown in Fig. 1. The heat capacity plot shows an anomalous divergence between 340 and 370 K for La_3NbO_7 and between 430 and 470 K for Nd_3NbO_7. The results confirmed a phase transition, similar to the results of Klimenko's study [36].

It was previously reported that Gd_3NbO_7 has a noncentrosymmetric to centrosymmetric transition based on the SHG measurement [44]. SHG measurements were also performed on La_3NbO_7 and Nd_3NbO_7. Fig. 2 shows the SHG signal of La_3NbO_7 as well as the SHG signal of Gd_3NbO_7 for comparison [44]. The laser power applied in measuring the SHG signals of La_3NbO_7 sample was 20 times higher than that used in measuring Gd_3NbO_7 sample. Only noise or white light generated by the laser was detected for La_3NbO_7. The same response was observed for Nd_3NbO_7, that is, no SHG signal was detected. Therefore, from these results, it can be inferred that La_3NbO_7 and Nd_3NbO_7 have centrosymmetric structures throughout the measured temperature range.

3.2. Synchrotron powder diffraction and neutron powder diffraction

3.2.1. Nd_3NbO_7

Synchrotron powder diffraction at 100 K and room temperature was performed on Nd_3NbO_7. The wavelength used was 0.40092 Å. The general reflection conditions for $Cmcm$ are $h+k=2n$ (n stands for integer) for ($h\,k\,l$) reflection and h, $l=2n$ for ($h\,0\,l$). There are 9 minor peaks that violate the reflection conditions for $Cmcm$ as shown in Fig. 3. By contrast, all the reflections are allowed for the general reflection conditions of $Pmcn$, which are $h+k=2n$ for ($h\,k\,0$) and $l=2n$ for ($0\,0\,l$). Therefore, it is clear that the correct space group of Nd_3NbO_7 below the phase transition temperature is $Pmcn$. To clarify, $Pmcn$ is a different setting of $Pnma$, which was chosen in previous studies [34,35]. The only difference between $Pmcn$ and $Pnma$ is the unit cell choice. The cell choice of (a, b, c) in $Pmcn$ corresponds to (c, a, b) in $Pnma$. The high temperature phase with the space group $Cmcm$ has the same unit cell choice as $Pmcn$. Therefore, in this study, $Pmcn$ is chosen to represent the low temperature phase. The synchrotron diffraction patterns were successfully refined with the space group $Pmcn$ using GSAS software [46,47]. Fig. 3 shows observed intensities, calculated intensities, and their differences of the whole pattern at room temperature with highlighting the $Cmcm$ forbidden peaks pointed by arrows.

Neutron diffraction ($\lambda=1.5378$ Å) was also collected on Nd_3NbO_7 at different temperatures. Below the phase transition

Table 2
Crystal data of Nd_3NbO_7 for the high temperature phase from the neutron diffraction. There are total 1832 reflections and 53 parameters refined. The wavelength is 1.5378 Å. The refined 2θ range is 10–130°.

450 K
Space group: $Cmcm$
10.9075(3) Å, 7.5240(2) Å, 7.6397(2) Å
$R_w=7.39\%$, $R_p=5.68\%$, $\chi^2=2.435$

	Wyckoff	x	y	z	U_{iso}
Nb	4c	0	0.5	0	0.011(1)
Nd1	4c	0	0	0	0.016(1)
Nd2	8g	0.2287(3)	0.2949(4)	0.25	0.0067(6)
O1	8d	0.1265(3)	0.3118(5)	0.9633(4)	0.0229(8)
O2	8d	0.1332(4)	0.0239(6)	0.25	0.0079(9)
O3	4c	0	0.4282(8)	0.25	0.018(1)

470 K
Space group: $Cmcm$
10.9083(3) Å, 7.5250(2) Å, 7.6405(2) Å
$R_w=6.71\%$, $R_p=4.91\%$, $\chi^2=4.054$

	Wyckoff	x	y	z	U_{iso}
Nb	4c	0	0.5	0	0.012(1)
Nd1	4c	0	0	0	0.0182(10)
Nd2	8g	0.2287(3)	0.2949(4)	0.25	0.0090(6)
O1	8d	0.1263(3)	0.3119(4)	0.9635(4)	0.0250(7)
O2	8d	0.1328(4)	0.0237(5)	0.25	0.0104(9)
O3	4c	0	0.4284(8)	0.25	0.020(1)

500 K
Space group: $Cmcm$
10.9100(3) Å, 7.5272(2) Å, 7.6421(2) Å
$R_w=7.22\%$, $R_p=5.5\%$, $\chi^2=4.39$

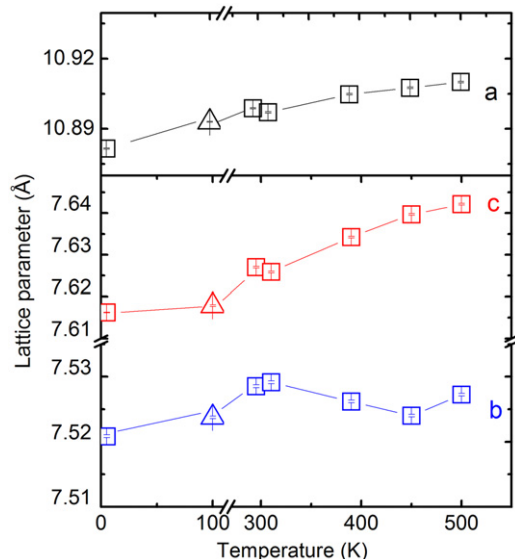|	Wyckoff	x	y	z	U_{iso}
Nb	4c	0	0.5	0	0.016(1)
Nd1	4c	0	0	0	0.019(1)
Nd2	8g	0.2288(3)	0.2956(4)	0.25	0.016(6)
O1	8d	0.1264(3)	0.3116(5)	0.9639(4)	0.0274(8)
O2	8d	0.1331(4)	0.0236(6)	0.25	0.014(1)
O3	4c	0	0.4288(8)	0.25	0.023(1)

Fig. 5. Lattice parameters of Nd_3NbO_7 at different temperatures. The solid square symbols indicate the lattice parameters from neutron diffraction. The open triangle symbols are from synchrotron powder diffraction.
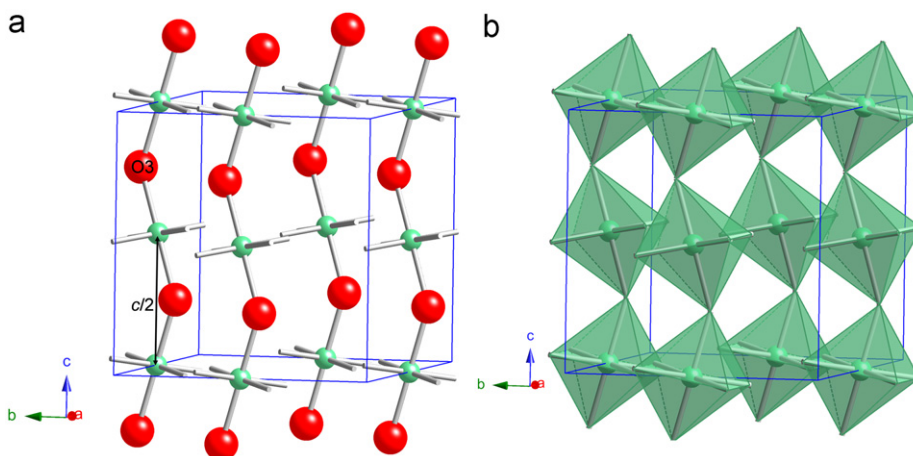
Fig. 6. (a) The Nb^{5+} ions align along [0 0 1]. The separate between two neighboring Nb^{5+} along the [0 0 1] direction is $c/2$. The O3 ions are shared by two neighboring Nb^{5+} ions and (b) polyhedra view of the NbO_6 octahedra. The NbO_6 octahedra align in a zigzag manner along [0 0 1].
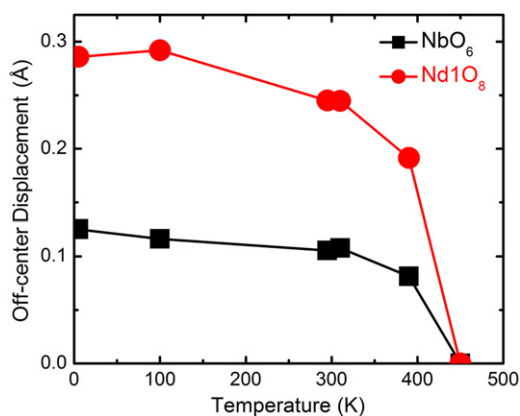

Fig. 7. Off-center displacements of Nb^{5+} inside NbO_6 and $Nd1^{3+}$ inside $Nd1O_8$ at different temperatures.

Fig. 8. The [0 0 1] view of the $Nd1^{3+}$ and Nb^{5+} ions for (a) the high temperature phase and (b) the low temperature phase. The blue lines stand for unit cell. The origin of the high temperature phase is (0.25, −0.25, 0) different from the low temperature phase. The ions in the second layer of (B) are indicated as solid black circle for better visual comparison. (For interpretation of the references to color in this figure legend, the reader is referred to the web version of this article.)

temperature ($\sim$450 K), the appearance of reflections (1 4 1) and (4 3 1) supports the space group $Pmcn$ (Fig. 4). The rest reflections, which supported the space group $Pmcn$ from synchrotron diffraction were overlapped or buried in the neighboring peaks in neutron diffraction patterns. The disappearance of (1 4 1) and (4 3 1) reflections above 450 K confirms the phase transition as shown in Fig. 4. The intensities of the (1 4 1) and (4 3 1) reflections are comparable at 5, 295, and 310 K and significantly decrease from 310 to 390 K. These two peaks totally disappear at 450, 470, and 500 K. Therefore, Nd_3NbO_7 undergoes a phase transition on heating from the space group $Pmcn$ to $Cmcm$.

The Rietveld refinement method was used to analyze all the neutron diffraction patterns with GSAS software [46,47]. The resulting atomic positions and isotropic atomic displacements are listed in Tables 1 and 2 (CSD-number 422631, 422632, 422633, 422634, 422635, 422636, 422637, and 422638). Fig. 5 indicates the lattice parameters after the refinements from both synchrotron and neutron diffractions. The room temperature lattice parameters match well with the previous study by Doi et al. [35]. There is an anomalous decrease of the lattice parameter b from 310 to 450 K. Similarly, Gd_3NbO_7 also exhibits a decrease in one lattice parameter from room temperature to the phase transition temperature [44]. Therefore, the anomalous decrease is consistent with a phase transition.

The phase refinement shows that above 450 K, Nb^{5+} ions occupy Wyckoff position $4b$ with site symmetry $2/m$ in the center of NbO_6 polyhedra (distorted octahedra). Each Nb^{5+} ion is bonded to four O1 (site symmetry 1) and two O3 (site symmetry $m2m$)
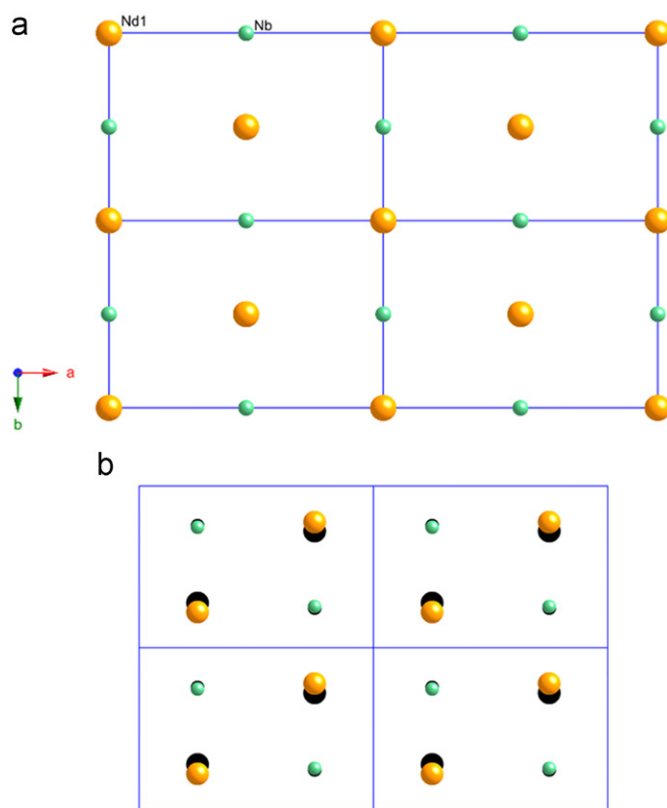
with O3 being corner-shared by neighboring NbO_6 polyhedra. The bond angle of O3–Nb–O3 is 180° (Fig. 6). The NbO_6 polyhedra align in a zigzag manner along [0 0 1] and the Nb^{5+} ions are separated with constant distance ($c/2$, c being the lattice parameter).

When cooling down to the transition temperature, the Nb^{5+} ions shift away from the center of the NbO_6 as well as the 2-fold axis. The shifts of ions are confined in the mirror plane, which is parallel to (1 0 0) and occupy a site with only mirror symmetry. The vectors between two neighboring Nb^{5+} ions are alternatively

[0, 2δ, −0.5] and [0, −2δ, −0.5] (δ is the shifting distance along [0 1 0] of Nb^{5+} ions). The shift of the Nb^{5+} ions away from the 2-fold axis also gives more freedom to the O^{2-} ions. As a result, the O3 ions shift away from the 2-fold axis parallel to [0 1 0] and the mirror plane parallel to (0 0 1) resulting in a site on the mirror plane parallel to (1 0 0). The O1 ions at the site symmetry 1 (Wyckoff position 16h) split into two unequal 8d with site symmetry 1 indicated as O1′ and O1″. Therefore, the NbO_6 polyhedra are more distorted since the O^{2-} ions have more degrees of freedom. The bond angle of O3–Nb–O3 cannot maintain 180°.

Similar to Nb^{5+}, the $Nd1^{3+}$ ions (site symmetry 2/m) at the center of $Nd1O_8$ polyhedra at the high temperature shifts away from the 2-fold axis and results in an off-center position (site symmetry m) at the low temperature. The off-center displacement of Nb^{5+} and $Nd1^{3+}$ generally decreases with increasing temperature as shown in Fig. 7. It is worth mentioning that due to the limitation of X-ray, the atomic positions of oxygen ions may not be exactly accurate at 100 K.

Fig. 8 shows the [0 0 1] view of the $Nd1^{3+}$ and Nb^{5+} ions both above and below the phase transition temperatures. In the high temperature phase, the $Nd1^{3+}$ ions as well as the Nb^{5+} ions align perfectly along the [0 0 1] direction. In the low temperature phase, the neighboring $Nd1^{3+}$ ions in the [0 0 1] direction shifts alternatively in [0 1 0] and [0 −1 0]. The neighboring Nb^{5+} ions in the [0 0 1] direction also moves away from the 2-folder axis alternatively in [0 1 0] and [0 −1 0]. There is no displacement along [1 0 0] for both types of the ions.

A more detailed comparison between the high temperature and low temperature phases is shown in Fig. 9. The high temperature phase indicated as the black circles is overlapped with the low temperature phase shown as the rendered spheres. It is clear that two neighboring Nb^{5+} ions or two adjacent $Nd1^{3+}$ ions along [0 0 1] displace in an antiparallel manner parallel to [0 1 0]. Because of the antiparallel manner, the net dipoles produced by the off-center displacement are compensated to zero. The neighboring Nb^{5+} and $Nd1^{3+}$ ions along [0 1 0] displace in the same direction, either in [0 1 0] or [0 −1 0].

It is worth mentioning that there is one extra peak at $d = 2.17$ Å, which cannot be indexed based on the orthorhombic lattice. This peak appears above or below the phase transition

temperature. The relative intensity is about 7% for neutron diffraction and below 0.15% for synchrotron diffraction (the peak cannot be detected by Cu$K\alpha$ XRD). The theoretical diffraction patterns of possible compounds like Nd_2O_3, $Nd(OH)_3$, $NdNbO_4$, $LaNb_5O_{14}$ (given the similarity of possible $NdNb_5O_{14}$), and $PrNb_3O_9$ (given the similarity of possible $NdNb_3O_9$) were compared with the un-indentified peak, but no clear match was obtained. The structure of Nd_3RuO_7 with a monoclinic lattice were also used as an initial crystal structure for Retieveld refinement [25]. However, it resulted in a poor refinement because the calculated pattern did not have a corresponding reflection for the un-indentified peak and also had several strong extra reflections, which did not show in the observed pattern. Therefore, it is reasonable to assume the un-identified peak comes from an unreported neodymium niobate or a minor impurity.

3.2.2. La_3NbO_7

The same phase transition occurring in Nd_3NbO_7 has also been found in La_3NbO_7. The refined atomic positions at different temperature are listed in Table 3 (CSD number 422626, 422627, and 422630) and Table 4 (CSD number 422628 and 422629). A summary of lattice parameters at different temperatures are shown in Fig. 10. The lattice parameter b shows anomalous extraction for the low temperature phase, the same as Nd_3NbO_7 and Gd_3NbO_7. After the phase transition temperature, the lattice parameter increases with increasing temperature. The $La1^{3+}$ and Nb^{5+} ions undergo off-center displacements of their corresponding polyhedra. The off-center shifts of both $La1^{3+}$ and Nb^{5+} decreases with increasing temperature are shown in Fig. 11.

3.3. Summary and discussion

It is interesting to see that the off-center shift of 8-coordinated Ln^{3+} is largest in Nd_3NbO_7, intermediate in La_3NbO_7, and smallest in Gd_3NbO_7 (Fig. 12). It can be inferred that it takes more thermal energy for Nd^{3+} to be able to move to the center of the corresponding polyhedra. Therefore, it makes sense that Nd_3NbO_7 has the highest phase transition temperature, La_3NbO_7 the second highest, and Gd_3NbO_7 the lowest.

It is important to notice that the phase transition is not only crystallographically interesting but also influential in physical properties. The temperature where the maximum of the real part of permittivity occurs at 1 MHz is close to the phase transition temperature in Fig. 13. It is strong evidence that the phase transition has impacts on dielectric properties. It is of importance to see that at 20 K the permittivity of these three compounds is almost the same, about 32. Nd_3NbO_7 has the highest difference in permittivity ($\Delta\varepsilon'_r$ in Fig. 13) while Gd_3NbO_7 has the lowest difference. The $\Delta\varepsilon'_r$ is also presented in Fig. 14. It increases with increasing off-center shifts of $Ln1^{3+}$. This very interesting finding may lead to potential avenues towards predicting/controlling the dielectric properties by knowing/modifying the structure.

As mentioned before, phase transition is commonly observed in Ln_3BO_7 compounds. The phase transition temperatures for Ln_3BO_7 are summarized in Fig. 15. It is based on the summary by Nishimine et al. [31] The phase transition temperatures for La_3NbO_7 and Nd_3NbO_7 are also added to Fig. 15. It is clearly seen that the phase transition temperature is related to the ionic radius of Ln^{3+}. Within the same B^{5+} ion, the phase transition temperature decreases with increasing the ionic radius of Ln^{3+}. It is worth mentioning that the phase transition in Gd_3NbO_7 occurs at 340 K, which does not follow the general trend. It is because Gd_3NbO_7 belongs to another weberite-type structure. In addition, all the phase transitions in Fig. 15 except Gd_3NbO_7 are from a P-type lattice to the orthorhombic lattice with space group $Cmcm$. The phase transition in Gd_3NbO_7 is from $C222_1$ to $Cmcm$.
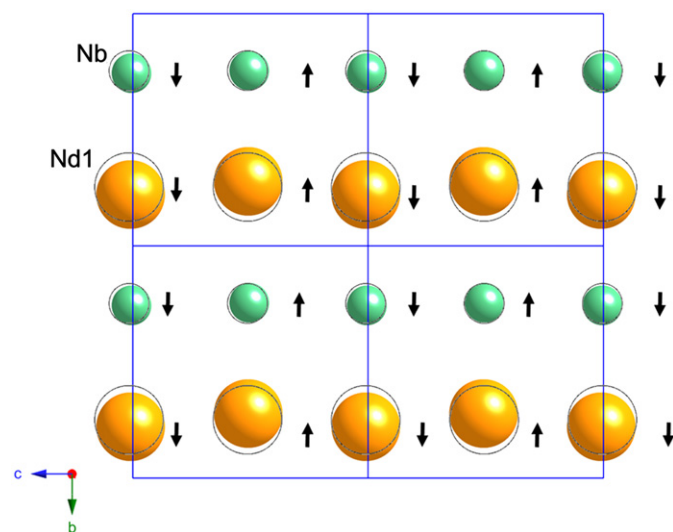

Fig. 9. The [1 0 0] view of spacing filling Nb and Nd1 chains parallel to the [0 0 1] direction, black circles show the center positions at high temperature phase. The black arrows above the atoms indicate the displacement orientation from the center positions along [0 1 0].

Table 3

Crystal data of La_3NbO_7 for the low temperature phase. There are total 1832 reflections and 64 parameters refined. The wavelength is 1.5378 Å. The refined 2θ range is 10–130°.

	20 K Space group: *Pmcn* 11.1478(3) Å, 7.6413(3) Å, 7.7407(2) Å R_w=10.80%, R_P=8.07%, χ^2=7.240				
	Wyckoff	x	y	z	U_{iso}
Nb	4c	0.25	0.2584(15)	0.0067(19)	0.008(1)
La1	4c	0.25	0.7762(9)	0.0073(12)	0.0079(15)
La2	8d	0.4748(3)	0.4498(5)	0.2528(13)	0.0063(7)
O1′	8d	0.1296(8)	0.4462(9)	0.5247(10)	0.010(2)
O1″	8d	0.3805(7)	0.4147(9)	0.9619(9)	0.0031(14)
O2	8d	0.3806(5)	0.7252(7)	0.253(2)	0.0074(11)
O3	4c	0.25	0.3206(9)	0.255(3)	0.0052(17)
	100 K Space group: *Pmcn* 11.1487(3) Å, 7.6398(3) Å, 7.7407(2) Å R_w=11.21%, R_P=8.2%, χ^2=7.806				
	Wyckoff	x	y	z	U_{iso}
Nb	4c	0.25	0.2601(16)	0.005(2)	0.0126(14)
La1	4c	0.25	0.7751(11)	0.0066(14)	0.018(2)
La2	8d	0.4750(4)	0.4487(5)	0.2515(15)	0.0157(8)
O1′	8d	0.8698(8)	0.9465(10)	0.9650(12)	0.020 (2)
O1″	8d	0.3806(8)	0.4156(9)	0.9621(11)	0.0126(17)
O2	8d	0.3807(5)	0.7258(7)	0.252(2)	0.0140(12)
O3	4c	0.25	0.3211(10)	0.253(3)	0.0143(18)
	295 K Space group: *Pmcn* 11.1593(4) Å, 7.6309(3) Å, 7.7522(2) Å R_w=10.19%, R_P=7.36%, χ^2=6.566				
	Wyckoff	x	y	z	U_{iso}
Nb	4c	0.25	0.2614(19)	0.001(2)	0.0132(15)
La1	4c	0.25	0.7696(14)	0.0086(17)	0.0179(18)
La2	8d	0.4754(4)	0.4492(5)	0.2512(18)	0.0169(9)
O1′	8d	0.8681(9)	0.9439(11)	0.9661(13)	0.021 (2)
O1″	8d	0.3797(8)	0.4196(10)	0.9615(13)	0.014(2)
O2	8d	0.3803(5)	0.7259(8)	0.250(3)	0.0150(13)
O3	4c	0.25	0.3196(10)	0.254(3)	0.0129(19)

Table 4

Crystal data of La_3NbO_7 for the low temperature phase. There are total 1832 reflections and 64 parameters refined. The wavelength is 1.5378 Å. The refined 2θ range is 10–130°.

|	380 K Space group: *Cmcm* 11.1667(4) Å, 7.6275(3) Å, 7.7588(2) Å R_w=9.74%, R_P=7.02%, χ^2=5.968				
	Wyckoff	x	y	z	U_{iso}
Nb	4b	0	0.5	0	0.0132(14)
La1	4a	0	0	0	0.0211(14)
La2	8g	0.2258(3)	0.3012(5)	0.25	0.0125(8)
O1	16h	0.1233(4)	0.3175(6)	0.9645(5)	0.0186(9)
O2	8g	0.1308(5)	0.0262(7)	0.25	0.0103(12)
O3	4c	0	0.4327(10)	0.25	0.0052(17)
	470 K Space group: *Cmcm* 11.1726(4) Å, 7.6336(3) Å, 7.7636(3) Å R_w=10.24%, R_P=7.61%, χ^2=6.642				
	Wyckoff	x	y	z	U_{iso}
Nb	4b	0	0.5	0	0.0171(17)
La1	4a	0	0	0	0.0241(17)
La2	8g	0.2262(4)	0.3009(5)	0.25	0.0163(9)
O1	16h	0.1233(4)	0.3177(6)	0.9652(6)	0.0245(11)
O2	8g	0.3699(6)	0.5267(8)	0.25	0.0149(14)
O3	4c	0	0.4336(11)	0.25	0.02(2)
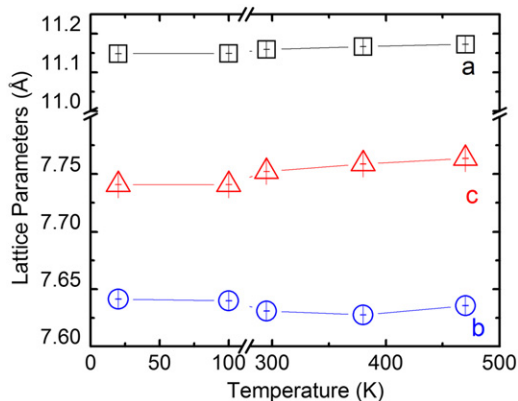
Fig. 10. Lattice parameters (with errors) of La_3NbO_7 at different temperatures.
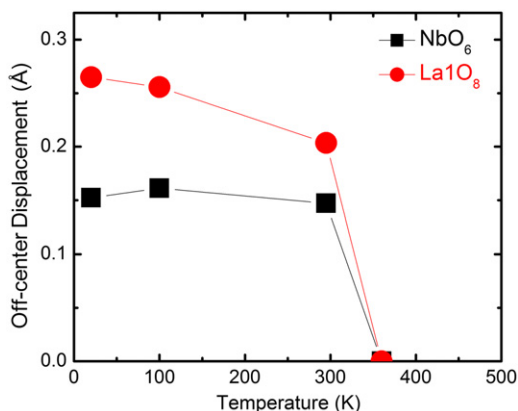

Fig. 11. Off-center displacements of Nb^{5+} inside NbO_6 and $La1^{3+}$ inside $La1O_8$ at different temperatures.
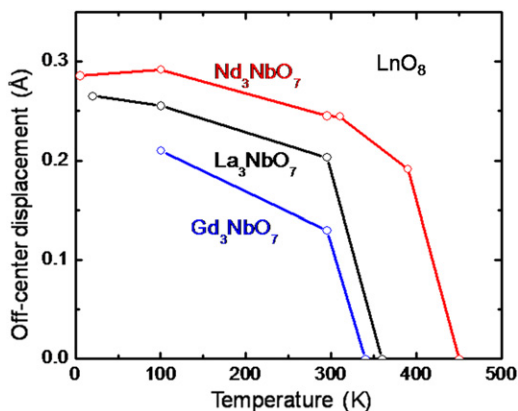

Fig. 12. Comparison of off-center displacement of LnO_8 at different temperature. The space group of the low temperature phase of Gd_3NbO_7 is $C222_1$.

Fig. 13. The real part of permittivity of La_3NbO_7 and Nd_3NbO_7. The figure also includes the real part of permittivity of Gd_3NbO_7 [10]. The arrows show the difference ($\Delta\varepsilon'_r$) between the maximum permittivity and the minimum permittivity.
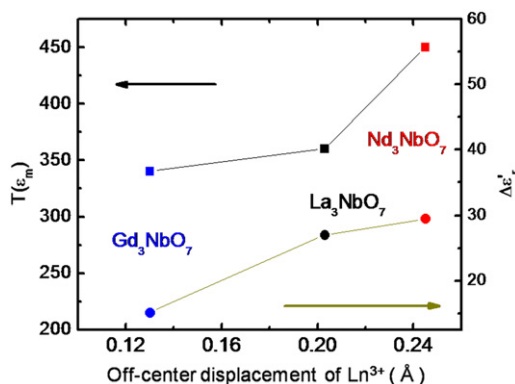

Fig. 14. $T(\varepsilon_m)$ and dielectric difference ($\Delta\varepsilon_r'$) from the maximum to the minimum vs. off-center displacement of Ln^{3+} inside $Ln1O_8$ polyhedra. $\Delta\varepsilon_r'$ is also indicated in Fig. 13.
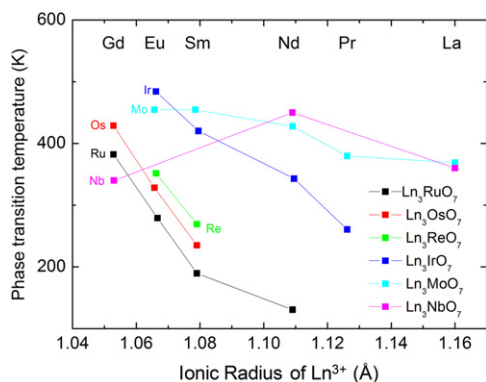

Fig. 15. Phase transition temperature for Ln_3BO_7. The figure is based on the summary by Nishimine et al. [31] and adds Ln_3NbO_7 points based on this work. The phase transition temperature of Ln_3RuO_7 and Ln_3OsO_7 is after Gemmill et al. [27,41], Ln_3MoO_7 and Ln_3IrO_7 after Nishimine et al. [5,31], Ln_3ReO_7 after Hinatsu et al. [4].

4. Conclusion

Heat capacity measurements and neutron diffraction confirmed a phase transition in Nd_3NbO_7 at about 450 K as well as in La_3NbO_7 at about 360 K. SHG measurements indicate that Nd_3NbO_7 and La_3NbO_7 have a centrosymmetric structure both below and above the phase transition temperature. Based on synchrotron diffraction and neutron diffraction of Nd_3NbO_7 and La_3NbO_7 at room temperature, the correct space group below the phase transition temperature was determined to be *Pmcn* as there are some minor peaks that violate the reflection conditions for

Cmcm. The disappearance of (1 4 1) and (4 1 3) reflections upon heating confirmed the phase transition from *Pmcn* to *Cmcm*. The Rietveld method was used to refine diffraction patterns at different temperatures. It was also concluded that the phase transition upon cooling is mainly due to the off-center shifts of Nb^{5+} and one third of the La^{3+} and Nd^{3+} ions within their corresponding polyhedra. The phase transition has impacts on the

dielectric properties. The difference in permittivity increases with increasing off-center shifts of $Ln1^{3+}$.

Acknowledgments

References

[1] M. Wakeshima, H. Nishimine, Y. Hinatsu, Journal of Physics Condensed Matter 16 (23) (2004) 4103–4120.

[2] H. Nishimine, M. Wakeshima, Y. Hinatsu, Journal of Solid State Chemistry 178 (4) (2005) 1221–1229.

[3] M. Wakeshima, Y. Hinatsu, Journal of Solid State Chemistry 179 (11) (2006) 3575–3581.

[4] Y. Hinatsu, M. Wakeshima, N. Kawabuchi, N. Taira, Journal of Alloys and Compounds 374 (1-2) (2004) 79–83.

[5] H. Nishimine, M. Wakeshima, Y. Hinatsu, Journal of Solid State Chemistry 177 (3) (2004) 739–744.

[6] R. Lam, F. Wiss, J.E. Greedan, Journal of Solid State Chemistry 167 (1) (2002) 182–187.

[7] J.R. Plaisier, R.J. Drost, D.J.W. IJdo, Journal of Solid State Chemistry 169 (2) (2002) 189–198.

[8] R. Lam, T. Langet, J.E. Greedan, Journal of Solid State Chemistry 171 (1-2) (2003) 317–323.

[9] L. Cai, J. Guzman, L. Perez, and J.C. Nino, Phase Formation and Dielectric Properties of Ln_3NbO_7 (Ln = Rare Earth Elements),in: Proceedings of Materials Research Society Symposium on Solid-State Chemistry of Inorganic Materials VI, 998E 0988-qq01-04, 2007.

[10] L. Cai, J.C. Nino, Journal of the European Ceramic Society 27 (13–15) (2007) 3971–3976.

[11] R. Abe, M. Higashi, Z.G. Zou, K. Sayama, Y. Abe, H. Arakawa, Journal of Physical Chemistry B 108 (3) (2004) 811–814.

[12] R. Abe, M. Higashi, K. Sayama, Y. Abe, H. Sugihara, Journal of Physical Chemistry B 110 (5) (2006) 2219–2226.

[13] L. Cai, J.C. Nino, Acta Crystallographica Section B—Structural Science 65 (2009) 269–290.

[14] S.S. Lopatin, L.N. Averyanova, I.N. Belyaev, Zhurnal Neorganicheskoi Khimii 30 (4) (1985) 867–872.

[15] G. Tilloca, Rev Int Hautes Temp 10 (3) (1973) 183–196.

[16] Y. Yamasaki, Y. Sugitani, Bulletin of the Chemical Soceity of Japan 51 (10) (1978) 3077–3078.

[17] H.J. Rossell, Journal of Solid State Chemistry 27 (1) (1979) 115–122.

[18] F.P.F. Vanberkel, D.J.W. Ijdo, Materials Research Bulletin 21 (9) (1986) 1103–1106.

[19] F. Wiss, N.P. Raju, A.S. Wills, J.E. Greedan, International Journal of Inorganic Materials 2 (1) (2000) 53–59.

[20] P. Khalifah, Q. Huang, J.W. Lynn, R.W. Erwin, R.J. Cava, Materials Research Bulletin 35 (1) (2000) 1–7.

[21] R.P. Bontchev, A.J. Jacobson, M.M. Gospodinov, V. Skumryev, V.N. Popov, B. Lorenz, R.L. Meng, A.P. Litvinchuk, M.N. Iliev, Physical Review B 62 (18) (2000) 12235–12240.

[22] W.A. Groen, F.P.F. Vanberkel, D.J.W. Ijdo, Acta Crystallographica Section C—Crystal Structure Communications 43 (1987) 2262–2264.

[23] P. Khalifah, R.W. Erwin, J.W. Lynn, Q. Huang, B. Batlogg, R.J. Cava, Physical Review B 60 (13) (1999) 9573–9578.

[24] D. Harada, Y. Hinatsu, Journal of Solid State Chemistry 164 (1) (2002) 163–168.

[25] D. Harada, Y. Hinatsu, Y. Ishii, Journal of Physics Condensed Matter 13 (48) (2001) 10825–10836.

[26] D. Harada, Y. Hinatsu, Journal of Solid State Chemistry 158 (2) (2001) 245–253.

[27] W.R. Gemmill, M.D. Smith, H.C. zur Loye, Inorganic Chemistry 43 (14) (2004) 4254–4261.

[28] Y. Yokogawa, M. Yoshimura, Journal of the American Ceramic Society 80 (8) (1997) 1965–1974.

[29] J.F. Vente, R.B. Helmholdt, D.J.W. Ijdo, Journal of Solid State Chemistry 108 (1) (1994) 18–23.

[30] J.F. Vente, D.J.W. Ijdo, Materials Research Bulletin 26 (12) (1991) 1255–1262.

[31] H. Nishimine, Y. Doi, Y. Hinatsu, M. Sato, Journal of the Ceramic Society of Japan 115 (1346) (2007) 577–581.

[32] G. Wltschek, H. Paulus, I. Svoboda, H. Ehrenberg, H. Fuess, Journal of Solid State Chemistry 125 (1) (1996) 1–4.

[33] J.G. Allpress, H.J. Rossell, J Solid State Chemistry 27 (1) (1979) 105–114.

[34] A. Kahnharari, L. Mazerolles, D. Michel, F. Robert, J Solid State Chemistry 116 (1) (1995) 103–106.

[35] Y. Doi, Y. Harada, Y. Hinatsu, Journal of Solid State Chemistry 182 (4) (2009) 709–715.

[36] A.N. Klimenko, V.M. Ionov, N.A. Tomilin, V.S. Sergeev, V.P. Sirotinkin, A.E. Prozorovskii, V.B. Rybakov, S.G. Zhukov, Zhurnal Neorganicheskoi Khimii 35 (3) (1990) 599–603.

[37] N. Barrier, P. Gougeon, Acta Crystallographica Section E—Structure Reports Online 59 (2003) I22–I24.

[38] J.E. Greedan, N.P. Raju, A. Wegner, P. Gougeon, J. Padiou, J Solid State Chemistry 129 (2) (1997) 320–327.

[39] N. Barrier, P. Gall, P. Gougeon, Acta Crystallographica Section C—Crystal Structure Communications 63 (2007) I102–I104.

[40] H. Nishimine, M. Wakeshima, Y. Hinatsu, J Solid State Chemistry 178 (4) (2005) 1221–1229.

[41] W.R. Gemmill, M.D. Smith, Y.A. Mozharivsky, G.J. Miller, H.C. zur Loye, Inorganic Chemistry 44 (20) (2005) 7047–7055.

[42] D. Harada, Y. Hinatsu, Y. Ishii, J Physics—Condensed Matter 13 (48) (2001) 10825–10836.

[43] N. Ishizawa, K. Tateishi, S. Kondo, T. Suwa, Inorganic Chemistry 47 (2) (2008) 560–566.

[44] L. Cai, D. Sava, V. Gopolan, J.C. Nino, Journal of the American Ceramic Society 93 (3) (2010) 875–880.

[45] ASTM E1269-05, Standard Test Method for Determining Specific Heat Capacity by Differential Scanning Calorimetry, ASTM International, 2005.

[46] A.C. Larson, R.B. Von Dreele, General Structure Analysis System (GSAS), Los Alamos National Laboratory Report, LAUR 86-748, 1994.

[47] B.H. Toby, Journal of Applied Crystallography 34 (2001) 210–213.